Food Research International 165 (2023) 112529

Contents lists available at ScienceDirect

Food Research International

journal homepage: www.elsevier.com/locate/foodres

Integrated design of micro-fibrous food with multi-materials fabricated by uniaxial 3D printing

Su Hyun Lee, Hyun Woo Kim *, Hyun Jin Park *

Department of Biotechnology, College of Life Science and Biotechnology, Korea University, Seoul 02841, Republic of Korea

ARTICLE INFO

Keywords:
3D food printing
Multi-material
Hybrid meat product
Fiberization
Surimi
Soy protein isolate
Potato starch

ABSTRACT

Owing to the interest in sustainable foods, a new approach known as 3D food printing is being employed to make fibrous foods for meat and fish substitutes. In this study, we developed a filament structure with a multi-material ink comprising fish surimi-based ink (SI) and plant-based ink (PI), using single-nozzle printing and steaming. PI and an SI + PI mix collapsed after printing owing to their low shear modulus, although both PI and SI showed gel-like rheological behaviors. However, unlike the control, the objects printed with two and four columns per filament remained stable and fiberized after steaming. Each SI and PI sample gelatinized irreversibly at approximately 50 °C. The different rheological values of these inks after cooling resulted in relatively strong (PI) and weak (SI) fibers, which constructed a filament matrix. A cutting test demonstrated that the transverse strength of the fibrous structure of the printed objects was higher than the longitudinal strength, in contrast to that of the control. The degree of texturization increased with the fiber thickness based on the column number or nozzle size. Thus, we successfully designed a fibrous system using printing and post-processing and substantially broadened the application opportunities for creating fibril matrices for sustainable food analogs.

1. Introduction

Owing to a greater awareness of the climate crisis and animal welfare, meat alternatives have been proposed as a solution for a sustainable food industry incorporating vegan food. In response to this adoption of an animal-free diet, the demand for plant-based meat analogs has escalated (Bryant & Sanctorum, 2021; Saget et al., 2021; Singh et al., 2021). Moreover, from a nutritional perspective, plant-based meat analogs can prevent high intake of cholesterol and saturated fatty acids due to meat consumption and reduce body fat in overweight individuals (Najjar & Feresin, 2019; Wild, 2016). Therefore, considerable research has been conducted on meat analogs derived from various plant-based protein sources such as soy, peas, wheat, and nuts (Fresán et al., 2019; Ismail et al., 2020; Tan et al., 2021). Recently, extrusion processes have been applied to produce textured meat analogs; however, product developers and researchers are faced with the challenge of mimicking natural meat structural systems, especially fibrous textures (Kyriakopoulou et al., 2019). Generally, extruded meat analogs are less juicy and have a poor fibrous structure (Sun et al., 2021). To overcome these limitations, extrusion-based 3D printing technology has been suggested for the design of meat substitutes (Fresán et al., 2019).

3D food printing is a novel approach for preparing fibrous foods, such as meat and seafood substitutes, to improve their structure or sensory properties (Boukid, 2021; Chao et al., 2022; Hema et al., 2020; Wang & Liu, 2021). Several studies have also been conducted to design nutritionally improved or texture-modified foods (Kouzani et al., 2017; Shahbazi et al., 2021). However, there are few published studies on the enhancement of meat structure design, such as fiber texturization using multi-materials. Ko et al. (2021) investigated soy protein-based alternative meat with hydrocolloid insertion, prepared via co-axial nozzle printing, as muscle fiber. Dual-extrusion printing has also been employed in many studies. This printing method allows for the creation of various sections in foods (Hertafeld et al., 2019; Liu et al., 2018). Dick et al. (2019) suggested incorporating a multi-layer fat in meat products using dual-head extrusion printing. Co-axial meat fiber synthesis or multiple printing with dual head produces texturized meat; however, such meat has some limitations in its application as a meat analog. These types of printing methods require additional devices, such as a multi-head or another ink cartridge for a co-axial nozzle. It is also difficult to manage an adequate ratio of muscle to fiber content. Moreover, in co-

Abbreviations: SI, fish surimi-based ink; PI, plant-based ink; SPI, soy protein isolate.

* Corresponding authors.
E-mail addresses: mn4012@korea.ac.kr (H.W. Kim), hjpark@korea.ac.kr (H.J. Park).

https://doi.org/10.1016/j.foodres.2023.112529
Received 18 August 2022; Received in revised form 12 January 2023; Accepted 21 January 2023
Available online 26 January 2023

axial printing, it is challenging to control the sophisticated thickness of wall materials. In this study, we investigated multi-material 3D printing through a uniaxial nozzle for the preparation of fibrous food, which can be a solution to the aforementioned challenges without the need for additional accessories or skills.

We selected a hybrid meat formulation for the fibrous food system, which is a next-generation meat substitute composed of both animal and plant proteins (Hartmann & Siegrist, 2017; Wang et al., 2022). Compared to conventional meat, a hybrid meat product can improve consumer perception from a sustainable viewpoint and provide more nutritional benefits (Chandler & McSweeney, 2022). We used fish surimi-based ink (SI) as the animal source along with plant-based ink (PI) to make a fibrous structure. Soy protein isolate (SPI) and potato starch were chosen as plant-based sources; they have been mainly used for printing ink and as substitutes for plant-based meat analogs (Chen et al., 2019a; Rowat et al., 2021). Fish surimi shows promise as a printing material for food printing owing to its elasticity and shear-thinning behavior, which is suitable for flowing out from a nozzle (Shi et al., 2022; Wang et al., 2018).

Several studies have investigated the synergistic effects of surimi and SPI or starch-based materials (Jafarpour et al., 2012). However, there have been few studies on the use of each filament in printing with heterogeneous ink reservoirs. The objective of this study was to investigate micro-unit fibers using multi-materials with uniaxial extrusion, which can produce a co-axial printing effect. Ink with properties of different materials was employed to derive a micro-fibrous food structure, in contrast to existing research focused on synthesizing homogeneous ink. Furthermore, we investigated the fibrous characteristics induced by cooking according to the printing parameters. Depending on the combination of the various inks used, this method can contribute to the production of meat or fish substitutes with various textures.

2. Materials and methods

2.1. Raw materials

Fish surimi paste and potato starch were purchased from Jineojeon-Kamabokko Co. (Gyeonggi-do, Korea) and Mok-Hwa Food Co. (Chuncheongnam-do, Korea), respectively. SPI and κ-carrageenan were obtained from ES Food Materials (Gyeonggi-do, Korea). Sodium chloride (extra-pure grade, F.W. 58.44) was provided by Ducksan Chemicals (Gyeonggi-do, Korea). Methyl cellulose (4000 cP) was obtained from Showa Chemical Industry Co., Ltd. (Tokyo, Japan).

2.2. Food-based ink preparation

2.2.1. SI and PI formulation

SI and PI with the formulations shown in Table 1 were prepared at 25 ℃. For SI, fish surimi paste was thawed in flowing water for 30 min, placed in a blender (Tefal Perfect Mix + BL811DKR, Group SEB Korea, Korea), comminuted for 1 min, and then passed through a 500 mm sieve. Subsequently, 97.5 % of the sieved surimi paste was thoroughly mixed with 0.5 % κ-carrageenan and 2 % NaCl.

For PI preparation, 8 % SPI, 7 % potato starch, and 3 % methylcellulose were firstly mixed. Then, 82 % distilled water was poured into the powder mixture and kneaded for 10 min to obtain a homogeneous paste. To enhance visualization from printing performance, 150 μL of rose pink food dye (Liqua-gel® food color, Chefmaster, USA) was added and mixed to 100 g PI. Both inks were placed in a 50 mL cylinder-shaped mold and frozen at − 23 °C for 1 h.

Table 1
Surimi and plant-based ink formulation for printing.

Ink type	Materials	wt (%)
Surimi-based ink (SI)	Fish surimi	97.5
	κ-carrageenan	0.5
	NaCl	2
Plant-based ink (PI)	Soy protein isolate	8
	Potato starch	7
	Methylcellulose	3
	Distilled water	82

2.2.2. Filament preparation for 3D printing

Frozen SI and PI were cut in half or quarter (for two or four columns, respectively), recombined according to Fig. 1a, and transferred into 50 mL syringes. The control was prepared by filling syringes with a uniform mixture of SI and PI (SI:PI at 1:1 v/v). All the inks in syringes were stored in a refrigerator at 4 °C overnight before measurement.

2.3. Rheological properties

The dynamic viscoelastic properties of SI and PI were investigated using a rheometer (Paar Physica MCR 302, Anton Paar, Austria) with a 25 mm (PP25/S) diameter and a 1.0 mm gap. All samples loaded in the rheometer were allowed to rest for 10 min before commencing the analysis. For the angular frequency sweep test and shear modulus, the sample surface exposed to air was coated with corn oil to prevent drying during the test.

2.3.1. Small-amplitude oscillatory shear (SAOS) and temperature sweep test

Strain sweep tests were performed at 10 rad/s to obtain the linear viscoelastic region (LVR) before the SAOS test. In the sweep test, the yield point (τ_y) was found as the shear rate at the limit of LVR and the flow point (τ_f) as the crossover point where $G' = G''$. Yield point and LVR were measured from the strain sweep test using same software, and flow point was analyzed using OriginPro 2018 (OriginLab Corporation, Northampton, MA, USA). The amplitude sweep test was performed at a constant deformation of 0.05 % strain within the LVR. The angular ramp was programmed from 1 to 100 rad/s to measure the storage (G') and loss (G'') moduli. The tests were conducted at 25 °C.

The thermal behavior and gelation properties of the inks were determined using a temperature sweep test. This test was also conducted at 0.05 % strain with a frequency range of 25–100 rad/s to measure the G' and G'' values. Each sample was programmed to heat from 20 to 100 °C and cool back to 20 °C at a rate of 8 °C/min.

2.3.2. Shear modulus

A time sweep of 200 s over a variable range of strains from 0.001 to 10 % at 25 °C was performed to determine the shear modulus of samples. The shear modulus was calculated from the slope of the shear stress vs. shear strain plot in the LVR.

2.4. Extrudability

The printing extrudability of pastes based on column and nozzle sizes was measured using the methods described by Jo et al. (2021) with slight modifications. The prepared 30 mL inks were placed in a 50 mL syringe reservoir, which was used as an extrusion cell. The reservoir diameter was 29 mm, and three nozzle sizes (1.0, 1.5, and 1.95 mm) were used. A compression test was performed with a 1.0 mm/s pre/post-test speed, 10.0 g trigger force, and 20.0 mm target distance using a texture analyzer (TA-XT Plus 50, Stable Micro Systems Ltd., UK) to analyze extruded hardness. The maximum force from the force–time curve was selected as the extruded hardness.

2.5. Printability of inks

A 3D printing test was performed using an extrusion-based 3D food printer (YOLI-LAB, YOLILO Co., Ltd., Korea) at 25℃.The printing speed was set as 25 mm/s. The printability of SI and PI was assessed as described by Kim et al. (2017) with a slight modification. A cylindrical

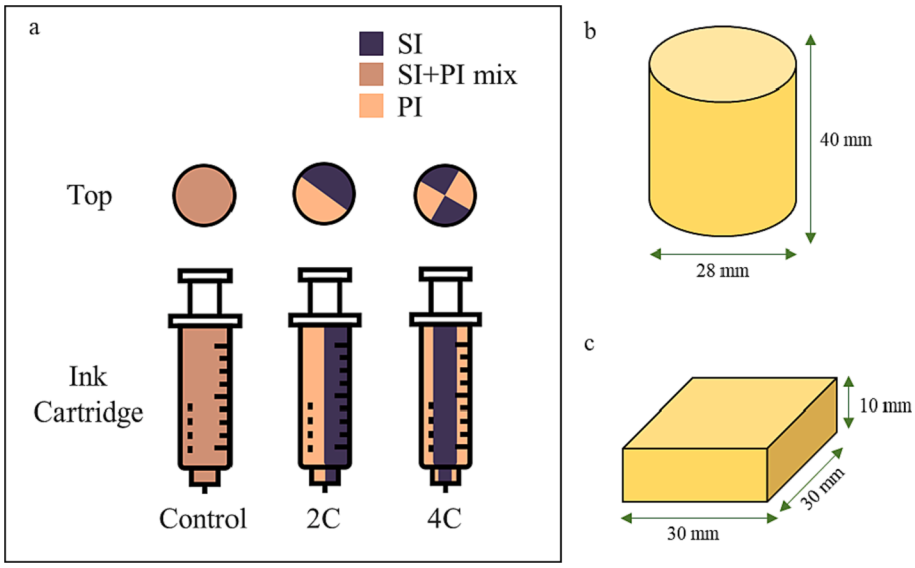

Fig. 1. Filament column design in an ink cartridge (**a**), 3D modeling for printability test (**b**), and fibrous structure system (**c**). In Panel **a**, 2C stands for two filling columns and 4C stands for four filling columns in the cartridge.

shape with dimensions of 28 mm (diameter) × 40 mm (height) was utilized as the target geometry, as shown in Fig. 1b, and the height of shape (40 mm) was selected as printability parameter to assess the printability of SI and PI. The dimensional stability (%) was calculated from the height (mm) after printing within 30 min divided by the designed height (40 mm).

2.6. Designing micro-fibrous structure of 3D printed product

A cuboid shape with a 35 mm length/width and 10 mm height (Fig. 1c) was used to create fibrous products. Three nozzle diameters (1.1, 1.5, and 1.95 mm) were used as printing parameters. Other printing conditions were used according to the ink printability test. The printed products were steamed for 40 min immediately after printing for post-processing (Kong et al., 2023). The cooking temperature was about 98℃ by measuring a digital infrared thermometer (GM320, Benetech, USA) while measuring the printed products. After steaming, the samples were cooled immediately in a refrigerator at 4 °C for 20 min. The next experiment was then conducted.

2.7. Analysis of texture of 3D printed objects

Texture profile analysis (TPA) and cutting tests were conducted to determine the mechanical properties of 3D steamed objects based on different nozzle and column sizes. The dimensions for measurement were 35 mm × 35 mm × 10 mm, as previously described. Mechanical characterization was performed using a texture analyzer (TA-XT Plus 50).

TPA was performed twice by 30 % compression, with a difference of 5 s between cycles. The crosshead attached to a P/100 flat probe was moved at a speed of 1 mm/s, and the trigger force was 5.0 g. The shear force of the fibrous samples was determined according to the method described by Dincer and Çakli (2015), with slight modifications. A texture analyzer with a V-shaped Warner–Bratzler blade probe was used to measure the cutting strength. The test was conducted with a 5 mm compression distance at a speed of 1 mm/s. The maximum force from the force–time curve was considered the shear force. The cutting strength of steamed objects was evaluated in two directions using fibers. The longitudinal strength (F_L) is that parallel to the fiber direction, and the transverse strength (F_T) is that perpendicular to the blades.

2.8. Statistical analysis

Analyses were conducted using three measurements to obtain the average values. SPSS 26.0 (IBM, Chicago, IL, USA) was used for statistical analyses. The significance of the treatment effects was estimated using one-way analysis of variance and Duncan's multiple comparison test. For all statistical analyses, significance was defined as $P < 0.05$.

3. Results and discussion

3.1. Rheological properties of SI and PI

The viscoelastic properties of SI, PI, and a mixture of SI and PI (SI + PI) are presented in Fig. 2. SAOS measurements have been widely used to identify the rheological behavior of food gels during gelation (Li et al., 2021). Relatively small strains within the LVR can induce rheological changes while maintaining the food network (Gunasekaran & Ak, 2000). Fig. 2a shows the stress sweep results for all three inks. The results showed that SI had the highest storage modulus (G′) and loss modulus (G″), followed by SI + PI, and then PI. The yield points (τ_y) of SI, SI + PI, and PI were 3434, 718, 579 Pa, respectively. τ_y value is the maximum amount of stress that can be applied before the deformation is irreversible, indicating the mechanical strength of maintaining deposited layers during the printing process (Prithviraj et al., 2022). On the other hand, in the flow point, SI + PI and PI held 3611 Pa and 6067 Pa, respectively, and followed by 15921 Pa of SI. τ_f implied the extrudability during printing, and the result indicated that SI need more force than PI or SI + PI for extrusion (Chen et al., 2019b).

As shown in Fig. 2b, it is notable that the G′ valuewas higher than the G″ valuefor all inks, which was corresponding to the strain sweep results. G indicates the elasticity of the food, whereas G″ represents the viscosity (Siacor et al., 2021). G′ affects mechanical, rupture strength, or adhesion, and it influences the ability of a printed object to support or maintain its shape and three-dimensional structure. On the other hand, G″ is related to the flow behavior of the food ink by affecting the extrusion operation during printing (Hussain et al., 2022; Yang et al., 2018). G′ of SI held 7541 ± 2268 Pa, which was bigger than G″ value, 2091 ± 585 Pa. G′ and G″ values were similar to a previous study by Kim et al. (2022). The other two inks exhibited a similar trend; SI + PI followed SI with a value of 2040 ± 983 Pa for G' and 816 ± 375 Pa for G″. Then the G' of PI was 973 ± 726 Pa and G″ was 595 ± 334 Pa. Hence, all inks exhibited solid-like, more elastic behavior, because their G′ was

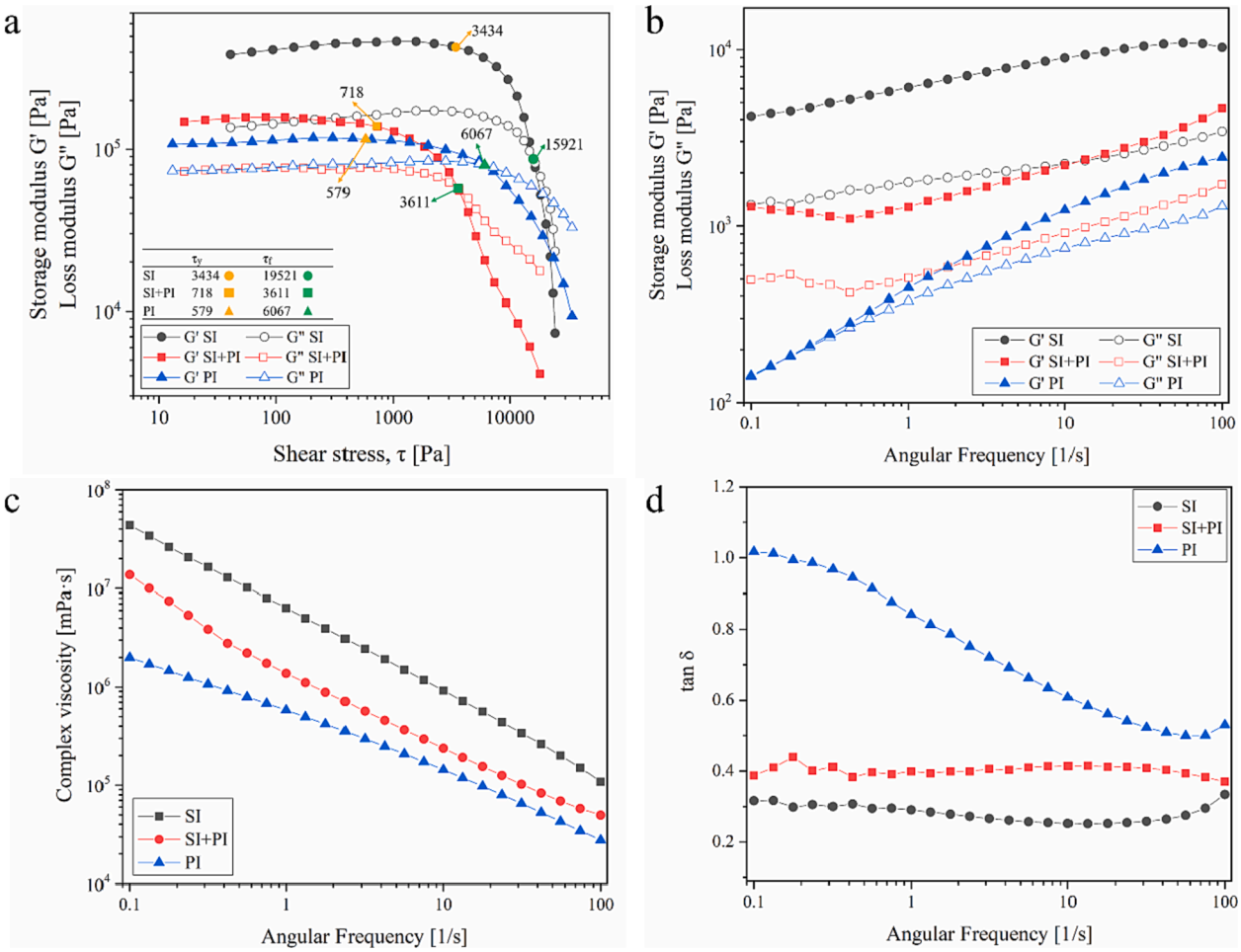

Fig. 2. Rheological properties of fish surimi-based ink (SI), plant-based ink (PI), and mixture (SI + PI). Stress sweeps for inks (a); yield point was expressed by yellow color, and the flow point was expressed by green color. Storage (G′) and loss (G″) moduli (b), complex viscosity (c), tan δ (d) from angular frequency sweep test. (For interpretation of the references to color in this figure legend, the reader is referred to the web version of this article.)

higher than G″. This rheological behavior helps retain the shape after printing and deposition on the printer surface (Jeon et al., 2021; Uribe-Wandurraga et al., 2020). SI has a stronger mechanical strength than PI owing to its higher G′ and G″ values in comparison with the other inks, indicating that SI exhibits better self-supportable performance, enabling shape stability, than PI (Liu et al., 2020).

PI was most dependent on the frequency, followed by SI + PI and SI. Since PI showed a steep gradient, it could be concluded that PI was more viscous than SI based on Newton's law of viscosity. Newton's viscosity law states that the shear stress owing to the viscosity of a fluid is proportional to the velocity gradient. Therefore, the resistance and frequency dependence decreases as the slope becomes gradual, indicating that PI is more viscous than SI, although both inks exhibit solid-like behaviors (Montoya et al., 2021).

Fig. 2cshows that the complex viscosity (η*) decreased with an increase in the angular frequency (ω) for all inks, indicating that they were shear-thinning fluids. The loss factor (tan δ) is shown in Fig. 2d, and tan δ was calculated as G″ divided by G′. The tan δ value of PI is approximately 1 in the low-frequency region, and the value decreases with an increase in the frequency. SI and SI + PI had lower tan δ values than PI, indicating that they exhibited better interface strength (Sriprablom et al., 2019). In summary, according to the angular frequency sweep test, SI exhibited more elastic behavior and was suitable for printing; therefore, it may serve as a support in the printing structure (Kim et al., 2021). However, PI is inappropriate for shape retention owing to its relatively low dynamic moduli.

3.2. 3D printing behaviors of SI and PI

We measured the shear modulus and dimensional stability to confirm the printability of SI and PI before making fibril-structured products. As shown in Fig. 3a, the shear modulus of SI was the highest (875.93 Pa), followed by those of SI + PI (138.57 Pa) and PI (80.10 Pa). Moreover, this tendency was consistent with the dimensional stability (98.72, 26.28, and 20.30 % for SI, SI + PI, and PI, respectively). The low shear modulus indicates that the mixture has poor dimensional stability, because it can easily collapse under its own weight after deposition owing to its softness (Kern et al., 2018; Zheng et al., 2021). Accordingly, it can be said that PI exhibits poor printing behavior compared to SI.

Fig. 3b shows the appearance of the printed objects after 30 min. SI exhibited good self-supporting properties, whereas PI and SI + PI collapsed after printing. This printability result may have been obtained due to the rheological properties of both inks. G′, which reflects the mechanical strength, is related to the dimensional stability, as it indicates the material resistance to shape deformation (Feng et al., 2019; Guo et al., 2021). SI + PI and PI collapsed after printing owing to their low shear and storage moduli, although both PI and SI exhibited solid-like behaviors.

3.3. Thermo-rheological behavior of SI and PI

The changes in G′ and G″ of SI and PI when heated from 20 to 100 °C at 1 °C/min were investigated using a temperature sweep test, as shown

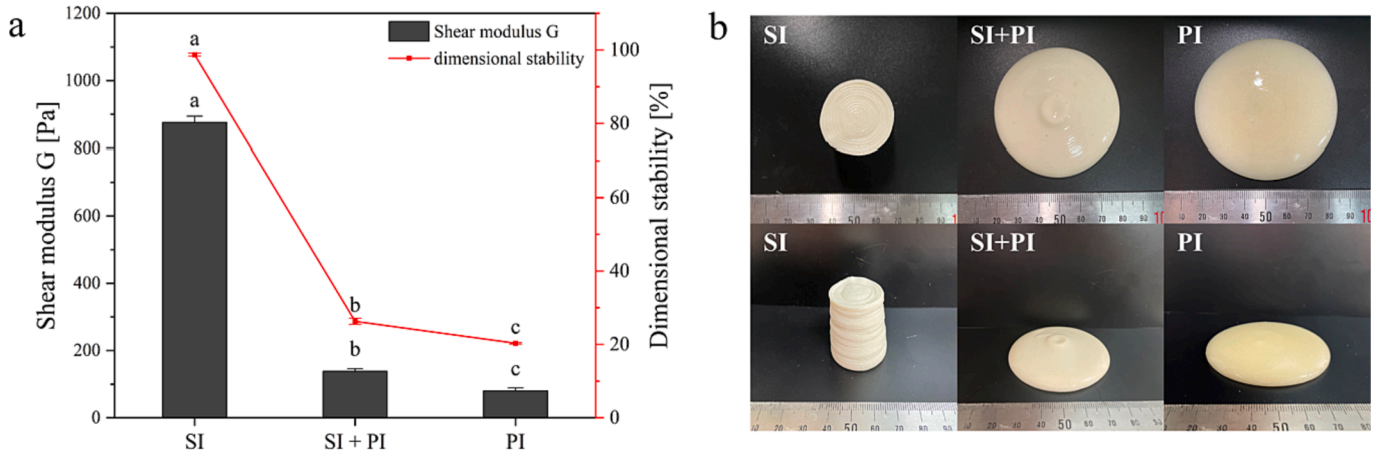

Fig. 3. Printing and thermal behavior of surimi-based ink (SI), plant-based ink (PI), and SI + PI. **a**: shape retention within 30 min after printing; **b**: visual appearance of SI, PI, and SI + PI printing results.

in Fig. 4. The initial G′ of SI was highest among those of the three inks, in accordance with the SAOS test (0.6803 Pa at 20 °C, followed by 0.4465 Pa for SI + PI and 0.2900 Pa for PI). All three inks showed thermosetting gelation behaviors, with sharp increases in G′ and G″, indicating a gel transformation, at approximately 40 °C when heated. However, after 60 °C, the order of the G′ and G″ values reversed, and PI showed the highest G′, followed by SI + PI and SI, whereas the G′ and G″ values of all three inks increased upon cooling. This was attributed to the interaction between potato starch and SPI in PI, resulting in heat-induced gelatinization. Several studies have investigated the interactions between starch and proteins involving hydrogen bonds and van der Waals forces (Colombo et al., 2011; Lu et al., 2016). Such interactions might result from higher crystallization due to the starch or protein ratio owing to greater compactness of the food system structure, which can be induced by hydrogen bonding with protein molecules (Villanueva et al., 2018).

SI derived from fish surimi, especially that of Alaskan pollock or common carp, is known for its sol–gel transition properties in the range of 40–60 °C, resulting in gel formation (Jafarpour & Gorczyca, 2009). Hunt and Park (2013) reported that the addition of κ-carrageenan along with salts to Alaskan pollock surimi improved its gel strength and water retention ability. This gelation might arise due to myosin, which contributes mainly to gel formation; sodium or potassium chloride solubilizes myosin, forming salt ion–myosin linkages, which are induced by heating (Lanier et al., 2005). Fish surimi with 2–2.5 % salt forms a

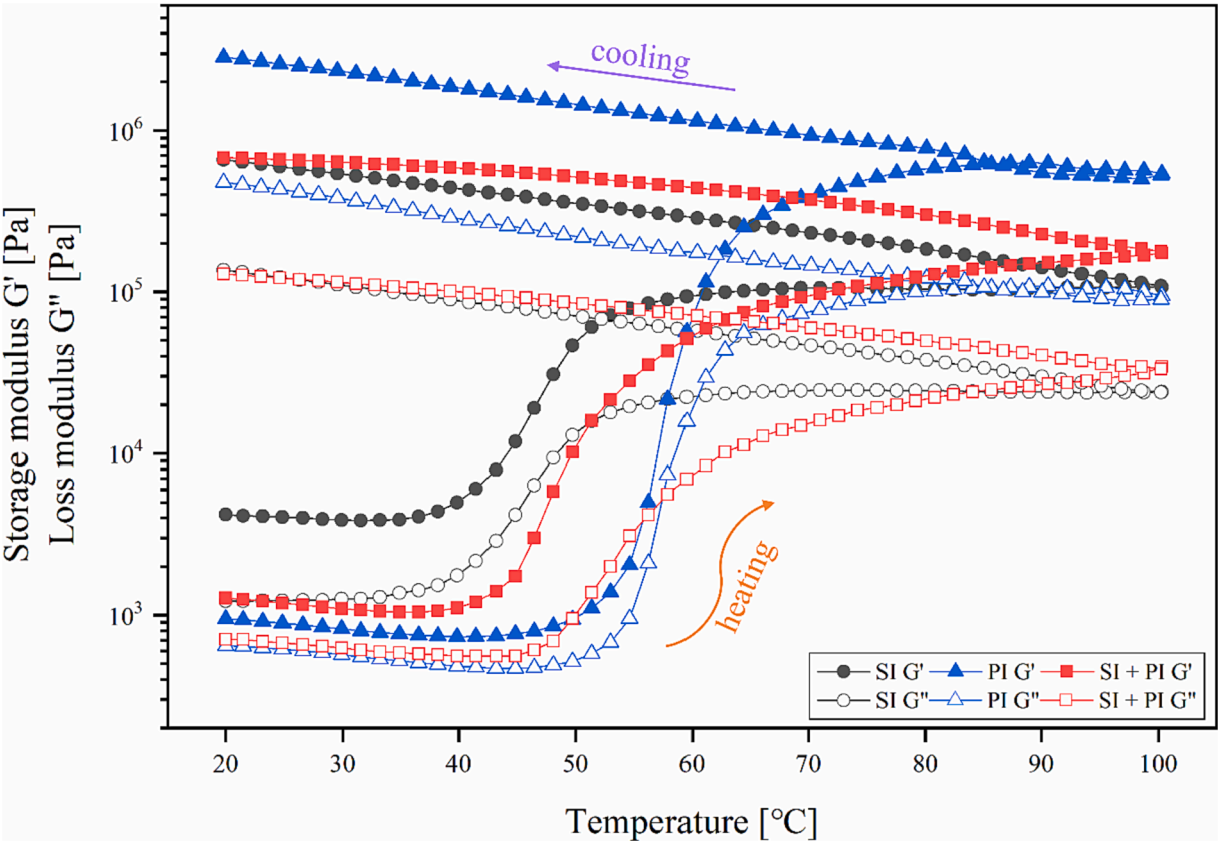

Fig. 4. Thermal gelation behavior of surimi-based ink (SI) and plant-based ink (PI). Storage (G′) and loss (G″) moduli versus temperature ramp (20 °C → 100 °C → 20 °C).

surimi gel upon heating; the gel strength can be increased by protein phosphorylation of surimi (Wang et al., 2018; Zhu et al., 2021).

PI was mainly composed of potato starch and SPI, and the ink represented the similar gelling behaviors of previous research. Torres et al. (2018) investigated thermo-rheological properties of native potato starch dispersion. The onset gelatinization temperature was about 45℃ and the final temperature was around 70℃. The potato starch gel was reinforced when cooling down to 25℃. On the other hand, protein addition influenced the starch gelling through the swelling degree of the potato starch granules since it might compete with the potato starch granules for the water molecules. However, the thermo-rheological behavior of potato starch with soy protein concentrate mixture demonstrated a similar trend to potato starch dispersion, and its gelatinization temperature was 77.1℃ in a previous study by Patraşcu et al. (2016).

SI + PI, which was a mixture of fish surimi, potato starch, and SPI, improved the gelation of surimi ink (Jafarpour et al., 2012). Overall, all three inks transformed into a cooked gel as the temperature increased, and PI had higher G′ and G″ values than SI after cooling, indicating better pasting and gel properties.

3.4. Fibrous structure of printed and cooked objects

Printed products were steamed as post-processing, and the steaming method has been selected as one of the post-processing treatments in recent years by researchers. (Thangalakshmi et al., 2022; Theagarajan et al., 2021). The cooked products with SI and PI formed gelation during steaming according to their thermo-rheological properties as shown in Fig. 4. Printed objects with two and four columns per filament were stable and fiberized after steaming, whereas the control with a homogenous mixture of SI and PI did not form a fibrous structure. Each SI and PI sample gelatinized irreversibly at approximately 50 °C, and the different rheological values of each ink after cooling resulted in relatively strong (PI) and weak (SI) fibers, which constructed a filament matrix.

The extruded hardness for each nozzle size and column group was investigated for handling properties such as printability before printing the objects. Fig. 5 shows that extrudability decreased with an increase in the nozzle size. The highest extruded force was 19438 g (1.1 mm group), followed by 11621 g for the 1.5 mm group and 7643 g for the 1.95 mm group. This is because printing extrusions with a smaller nozzle diameter requires a higher extrusion force (Chang et al., 2011; Fu et al., 2021). However, for the same nozzle size, there was no significant difference in extrudability because the ink composition in the reservoir was the same, except for the filling type. Nevertheless, all inks in the syringe attached with three different nozzles belonged to grade A (<3 kg of extruded hardness) based on the classification of extrudability reported by Kim et al. (2017), which presents easy-to-extrude handling properties and is applicable to sophisticated 3D objects.

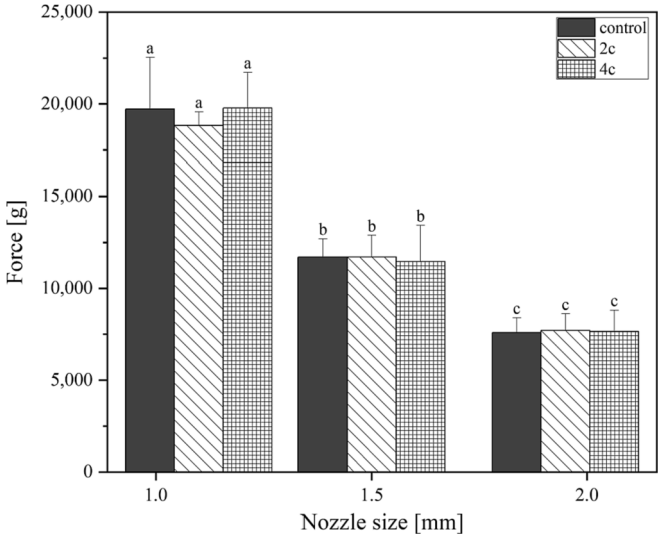

Fig. 5. Extruded hardness based on nozzle size and ink type; different letters indicate significant differences ($p < 0.05$).

Fig. 6 shows printed and steamed objects made with different nozzle and column diameters. Simultaneous printing with multi-materials is based on Pascal's principle, which states that the pressure in a static fluid at any point is evenly distributed in all directions. Hence, individual filaments can be formed by printing without mixing, similar to a closed toothpaste tube (Pisano, 2021). Because the control was printed with a mixture of SI and PI, it collapsed without being able to withstand the printing template height relative to the dimensional stability result investigated previously. However, the printed objects with columns maintained the shape of the printing template better because SI had good self-supporting characteristics. These results suggest that the final product can be self-supported by sufficiently supporting not only the fiber structure but also the material with low dimensional stability since the independent arrangement of materials has high printability in the multi-filament. In addition, a large-diameter nozzle printed relatively poor and coarse models, whereas a smaller nozzle diameter resulted in fine and compact models, consistent with the finding of Yang et al. (2018) that a smaller nozzle diameter resulted in a smoother surface in lemon juice gel printing.

We selected the steaming process after printing as the post-processing for printed objects owing to the gelation properties of surimi and potato starch-SPI. The printed objects that were not cooked were in paste form, and they did not make any linkages or fibers. However, after cooking, as shown in Fig. 6, when the objects were torn by hand in the fiber direction, the objects tore along the fibers, and a fibrous system was observed. In particular, fiber tearing occurred in the gap between the fibers or via SI, which formed a relatively weak fiber. This might be attributed to the lower G′ of SI after heating and cooling, according to previous temperature sweep test results.

3.5. Mechanical characterization of printed and post-processed products

3.5.1. Cutting strength

The shear forces in the transverse and longitudinal fiber directions were investigated. The fiber thickness had a notable influence on the shear force parameters, which improved the cutting strength. As shown in Fig. 7, all transverse cutting strengths, except that of the control group, were higher than the longitudinal strengths. This indicated that a fibrous structure formed in the samples printed with two or four columns. Osen et al. (2014) reported that a larger difference between F_T and F_L indicated a more fibrous texture, whereas similar values indicated a uniform system. In addition, the transverse cut requires more force because it is performed over the fibers rather than between the fibers, as for the longitudinal cut (Zahari et al., 2020). The transverse force (F_T) increased from 0.0525 to 0.0623 N/mm with an increase in the nozzle size in the 2C group and increased from 0.0436 to 0.0497 N/mm in the 4C group. In contrast, the results of cutting strength in the control group showed no significant difference between the longitudinal and transverse cuts, indicating that the steamed objects of the control group were not fibrous.

The force required for the transversal cut increased as the fiber was made thicker by a higher nozzle size or column number. These results were confirmed using the degree of texturization, which indicates fibrous structure formation, as presented in Table 2. The degree of texturization of all samples was greater than 1 and increased with the nozzle size in the same column group. A comparison of the column groups with the same nozzle diameter indicated that the degree of texturization of 2C was higher than that of 4C, indicating that objects with thicker filaments made the food structure tougher and increased the degree of texturization.

Fig. 6. The images of 3D printed and post-processed cuboid samples with various columns and nozzle diameters. The red coloring was added in PI. (For interpretation of the references to color in this figure legend, the reader is referred to the web version of this article.)

3.5.2. Texture profile analysis

The results of fibrous characteristics and TPA tests based on the column number and printing nozzle size are presented in Table 3. Compared to the degree of texturization shown in Table 2, the TPA parameters negatively correlated with the fiber thickness formulated according to the nozzle size or filling column. The fiber thickness had a notable influence on the TPA parameters, which improved the hardness.

A decrease in the nozzle size led to a gradual increase in hardness, except for that of the control, which may have been due to the presence of more compact fibers. Other TPA parameters, such as adhesiveness, springiness, cohesiveness, and chewiness, also decreased with an increase in the nozzle size. This was attributed to the more compact internal structure of the foods, induced by thinner filaments produced through the smaller diameter of the nozzle. There was no significant difference within the control group, and the results indicated that the control group did not have a fibrous structure, as shown in Fig. 5, or a high degree of texturization, as described previously.

All TPA parameters of the printed samples tended to be higher with four columns than with two columns. This trend was consistent when the fiber was thinner, the objects had a more compact structure, and the TPA parameters, including hardness, had higher values. If a food is more fibrous and has a smaller particle size owing to a thinner nozzle size, higher TPA parameters can be attributed to the increased surface area of the filament and the exposure of the fibers to friction. This might also be because, when the food was printed with a larger nozzle size, the resolution decreased, resulting in a more porous matrix. Similar results have been reported for the nozzle diameter effects of compression strength on printed carrot appetizer cakes (Guénard-Lampron et al., 2021).

The relationship between the hardness and texturization degree is represented in the scatter plot shown in Fig. 8. The concept of degree of texturization, calculated as F_T divided by F_L, was adopted from the extrusion processes described by Chen et al. (2010) and Marouene et al.

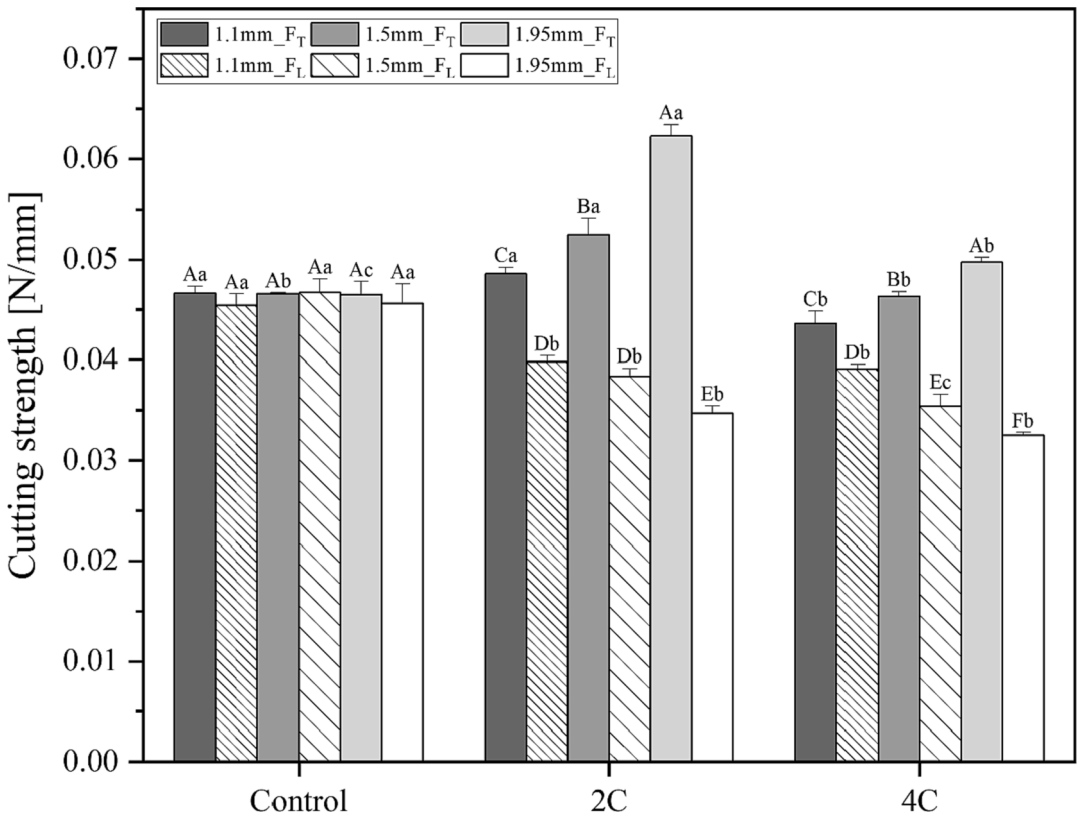

Fig. 7. Cutting strength of 3D-printed and post-processed objects. Different uppercase letters indicate significant differences within the same column group, and different lowercase letters indicate significant differences among the column groups in the same nozzle size and fiber direction ($p < 0.05$).

Table 2
Texture profile analysis of 3D printed and cooked objects with fibrous system.

Printing conditions		TPA parameters				
Column	Nozzle (mm)	Hardness (g)	Adhesiveness (g)	Springiness (g·sec)	Cohesiveness	Chewiness
Control	1.1	746.05 ± 28.63^{c}	-67.81 ± 12.53^{cd}	0.14 ± 0.00^{d}	0.14 ± 0.00^{ef}	14.42 ± 0.44^{d}
	1.5	740.88 ± 28.58^{c}	-44.31 ± 3.08^{e}	0.14 ± 0.00^{cd}	0.15 ± 0.00^{d}	15.88 ± 0.92^{d}
	1.95	730.52 ± 24.39^{c}	-58.01 ± 13.98^{de}	0.15 ± 0.00^{cd}	0.14 ± 0.01^{de}	15.14 ± 1.47^{d}
2C	1.1	914.91 ± 3.75^{b}	-119.14 ± 16.97^{a}	0.17 ± 0.00^{b}	0.18 ± 0.00^{b}	26.92 ± 0.41^{b}
	1.5	628.60 ± 3.98^{d}	-75.92 ± 3.67^{bc}	0.15 ± 0.00^{c}	0.16 ± 0.00^{c}	14.86 ± 0.72^{d}
	1.95	539.77 ± 10.92^{f}	-48.97 ± 2.46^{e}	0.13 ± 0.00^{e}	0.13 ± 0.01^{f}	9.43 ± 0.82^{f}
4C	1.1	981.79 ± 14.60^{a}	-121.84 ± 9.29^{a}	0.18 ± 0.01^{a}	0.20 ± 0.00^{a}	35.59 ± 1.70^{a}
	1.5	731.77 ± 6.79^{c}	-85.22 ± 4.79^{b}	0.16 ± 0.00^{b}	0.17 ± 0.00^{c}	19.91 ± 0.91^{c}
	1.95	574.67 ± 8.42^{e}	-48.85 ± 3.08^{e}	0.14 ± 0.00^{cd}	0.15 ± 0.01^{de}	11.87 ± 0.80^{e}

The values are the mean ± standard deviation of 3 replicates. Different small letters in the same column indicate significant difference ($p < 0.05$).

Table 3
The degree of texturization of 3D printed and cooked objects with fibrous system.

Column	Nozzle (mm)	Texturization degree
Control	1.1	1.03 ± 0.04^{f}
	1.5	1.00 ± 0.03^{f}
	1.95	1.02 ± 0.04^{f}
2C	1.1	1.18 ± 0.05^{d}
	1.5	1.37 ± 0.02^{c}
	1.95	1.79 ± 0.01^{a}
4C	1.1	1.12 ± 0.04^{e}
	1.5	1.31 ± 0.06^{c}
	1.95	1.53 ± 0.03^{b}

The values are the mean ± standard deviation of 3 replicates. Different small letters indicate significant difference ($p < 0.05$).

(2021). According to Fig. 8, hardness based on TPA inversely correlated with the degree of texturization, except in the control group. The objects cooked after extrusion through 1.95 mm 2C showed the highest degree of texturization and lowest hardness whereas those cooked after extrusion through 1.1 mm 4C had the lowest degree of texturization (not considering the control group) and the highest hardness.

4. Conclusion

In this study, we successfully designed a method for fabricating filament-structured food with inks of different properties using uniaxial 3D printing and demonstrated the relationship between the texture characteristics of printed foods and fiber compactivities based on printing nozzle size and filling column number. Based on a frequency sweep test, G' was greater than G" for SI, PI, and a mixture of SI and PI; both G' and G" of SI were greater than those of PI and SI + PI. The dimensional stability values of all inks were consistent with the

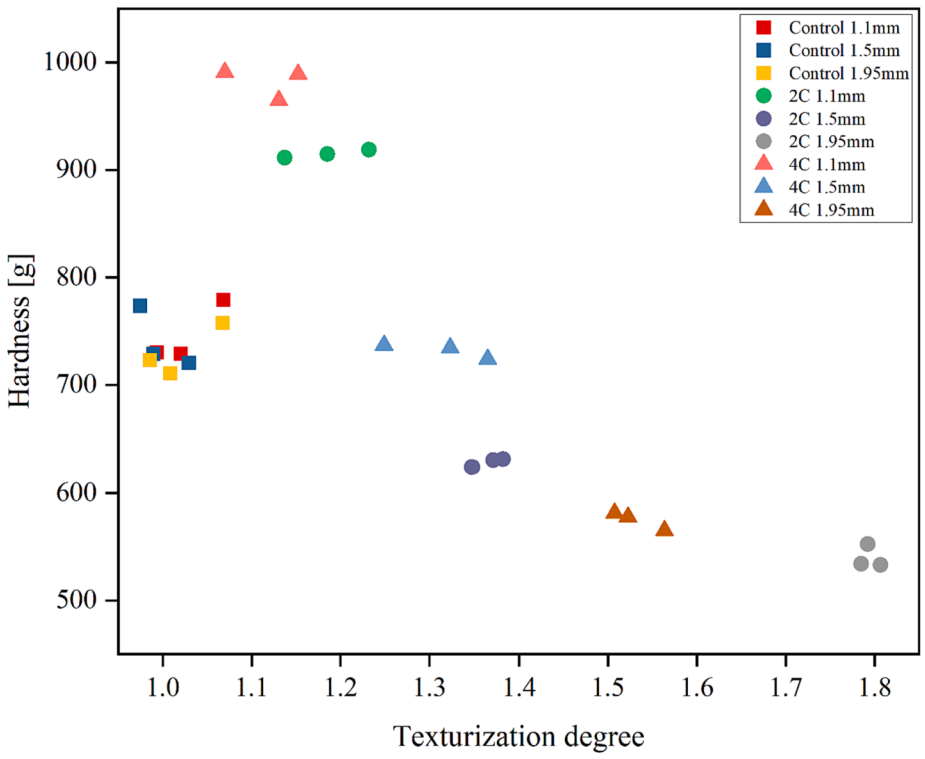

Fig. 8. Relationship between degree of texturization and hardness based on texture profile analysis of cooked objects.

frequency sweep test results. Printed objects with two or four columns were fiberized by steaming after printing. This was confirmed using a temperature sweep test. PI exhibited relatively higher G' and G" values than SI, indicating that PI acts as the core material in the fibrous structure. The cooked objects were well-texturized; the transverse cutting strength of all samples, except for the control, showed higher values than the longitudinal because the cutting blade was moved over the filaments, not between the filaments, such as for longitudinal cutting. The fiber thickness based on the nozzle size and column number, as well as the fiber direction, also impacted the cutting strength. This study has demonstrated the feasibility of fibrous printed foods with multi-materials using conventional extrusion-based 3D food printing. Thus, this approach may provide a guideline for modifying product textures like multi-head printing effects without any attachment. It also can be used for the printability improvement of materials having a low self-supporting ability. Moreover, hybrid meat can substantially broaden the application opportunities for preparing a fibril matrix for sustainable food analogs. It can also be applied to other 3D-printed foods that require a filament structure, such as inserts of various materials or meat analogs.

CRediT authorship contribution statement

Su Hyun Lee: Conceptualization, Methodology, Software, Validation, Formal analysis, Investigation, Writing – original draft. **Hyun Woo Kim:** Resources, Methodology, Writing – review & editing. **Hyun Jin Park:** Resources, Supervision.

Declaration of Competing Interest

The authors declare that they have no known competing financial interests or personal relationships that could have appeared to influence the work reported in this paper.

Data availability

No data was used for the research described in the article.

Acknowledgements

This work was supported by the Basic Science Research Program through the National Research Foundation of Korea (NRF) funded by the Ministry of Science, ICT & Future Planning [contract grant number NRF-2020R1A2C1011723]; collaborative research program between university and Rural Development Administration [PJ01527503 and PJ01591202], Republic of Korea; Samyang Igeon Scholarship Foundation in 2022. This research was also supported by a grant from the Institute of Biomedical Science & Food Safety, Korea University, Republic of Korea.

References

Boukid, F. (2021). Plant-based meat analogues: From niche to mainstream. *European Food Research and Technology, 247*(2), 297–308.

Bryant, C., & Sanctorum, H. (2021). Alternative proteins, evolving attitudes: Comparing consumer attitudes to plant-based and cultured meat in Belgium in two consecutive years. *Appetite, 161*, Article 105161.

Chandler, S. L., & McSweeney, M. B. (2022). Characterizing the properties of hybrid meat burgers made with pulses and chicken. *International Journal of Gastronomy and Food Science, 27*, Article 100492.

Chang, C. C., Boland, E. D., Williams, S. K., & Hoying, J. B. (2011). Direct-write bioprinting three-dimensional biohybrid systems for future regenerative therapies. *Journal of Biomedical Materials Research Part B: Applied Biomaterials, 98*(1), 160–170.

Chao, C., Hwang, J. S., Kim, I. W., Choi, R. Y., Kim, H. W., & Park, H. J. (2022). Coaxial 3D printing of chicken surimi incorporated with mealworm protein isolate as texture-modified food for the elderly. *Journal of Food Engineering, 111151*.

Chen, J., Mu, T., Goffin, D., Blecker, C., Richard, G., Richel, A., & Haubruge, E. (2019a). Application of soy protein isolate and hydrocolloids based mixtures as promising food material in 3D food printing. *Journal of Food Engineering, 261*, 76–86.

Chen, F. L., Wei, Y. M., Zhang, B., & Ojokoh, A. O. (2010). System parameters and product properties response of soybean protein extruded at wide moisture range. *Journal of Food Engineering, 96*(2), 208–213.

Chen, H., Xie, F., Chen, L., & Zheng, B. (2019b). Effect of rheological properties of potato, rice and corn starches on their hot-extrusion 3D printing behaviors. *Journal of Food Engineering, 244*, 150–158.

Colombo, A., León, A. E., & Ribotta, P. D. (2011). Rheological and calorimetric properties of corn-, wheat-, and cassava-starches and soybean protein concentrate composites. *Starch-Stärke, 63*(2), 83–95.
Dick, A., Bhandari, B., & Prakash, S. (2019). Post-processing feasibility of composite-layer 3D printed beef. *Meat Science, 153*, 9–18.
Dincer, M. T., & Çakli, Ş. (2015). Textural acceptability of prepared fish sausages by controlling textural indicators. *Turkish Journal of Veterinary & Animal Sciences, 39*(3), 364–368.
Feng, C., Zhang, M., & Bhandari, B. (2019). Materials properties of printable edible inks and printing parameters optimization during 3D printing: a review. *Critical Reviews in Food Science and Nutrition, 59*(19), 3074–3081.
Fresán, U., Mejia, M. A., Craig, W. J., Jaceldo-Siegl, K., & Sabaté, J. (2019). Meat analogs from different protein sources: A comparison of their sustainability and nutritional content. *Sustainability, 11*(12), 3231.
Fu, Z., Naghieh, S., Xu, C., Wang, C., Sun, W., & Chen, X. (2021). Printability in extrusion bioprinting. *Biofabrication, 13*(3), Article 033001.
Guénard-Lampron, V., Masson, M., Leichtnam, O., & Blumenthal, D. (2021). Impact of 3D printing and post-processing parameters on shape, texture and microstructure of carrot appetizer cake. *Innovative Food Science & Emerging Technologies, 72*, Article 102738.
Gunasekaran, S., & Ak, M. M. (2000). Dynamic oscillatory shear testing of foods—selected applications. *Trends in Food Science & Technology, 11*(3), 115–127.
Guo, C., Zhang, M., & Devahastin, S. (2021). Color/aroma changes of 3D-Printed buckwheat dough with yellow flesh peach as triggered by microwave heating of gelatin-gum Arabic complex coacervates. *Food Hydrocolloids, 112*, Article 106358.
Hartmann, C., & Siegrist, M. (2017). Consumer perception and behaviour regarding sustainable protein consumption: a systematic review. *Trends in Food Science & Technology, 61*, 11–25.
Hema, K., Velayutham, P., Mohan, C. O., Sukumar, D., Sundaramoorthy, B., Athithan, S., & Kumar, K. A. (2020). Innovative studies on "Analogue shrimp products" from lizard fish using 3D printing. *Indian Journal of Animal Research, 54*, 918–923.
Hertafeld, E., Zhang, C., Jin, Z., Jakub, A., Russell, K., Lakehal, Y., Andreyeva, K., Bangalore, S. N., Mezquita, J., & Blutinger, J. (2019). Multi-material three-dimensional food printing with simultaneous infrared cooking. *3D Printing and Additive Manufacturing, 6*(1), 13–19.
Hunt, A., & Park, J. W. (2013). A laska Pollock Fish protein gels as affected by refined carrageenan and various salts. *Journal of Food Quality, 36*(1), 51–58.
Hussain, S., Malakar, S., & Arora, V. K. (2022). Extrusion-based 3D food printing: Technological approaches, material characteristics, printing stability, and post-processing. *Food Engineering Reviews, 14*(1), 100–119.
Ismail, I., Hwang, Y.-H., & Joo, S.-T. (2020). Meat analog as future food: A review. *Journal of Animal Science and Technology, 62*(2), 111.
Jafarpour, A., & Gorczyca, E. M. (2009). Rheological characteristics and microstructure of common carp (*Cyprinus carpio*) surimi and kamaboko gel. *Food Biophysics, 4*(3), 172–179.
Jafarpour, A., Hajiduon, H.-A., & Aie, M. (2012). A comparative study on effect of egg white, soy protein isolate and potato starch on functional properties of common carp (*Cyprinus carpio*) surimi gel. *Journal of Food Processing and Technology, 3*(11).
Jeon, W. Y., Yu, J. Y., Kim, H. W., & Park, H. J. (2021). Production of customized food through the insertion of a formulated nanoemulsion using coaxial 3D food printing. *Journal of Food Engineering, 311*, Article 110689.
Jo, G. H., Lim, W. S., Kim, H. W., & Park, H. J. (2021). Post-processing and printability evaluation of red ginseng snacks for three-dimensional (3D) printing. *Food Bioscience, 42*, Article 101094.
Kern, C., Weiss, J., & Hinrichs, J. (2018). Additive layer manufacturing of semi-hard model cheese: Effect of calcium levels on thermo-rheological properties and shear behavior. *Journal of Food Engineering, 235*, 89–97.
Kim, H. W., Bae, H., & Park, H. J. (2017). Classification of the printability of selected food for 3D printing: Development of an assessment method using hydrocolloids as reference material. *Journal of Food Engineering, 215*, 23–32.
Kim, S. M., Kim, H. W., & Park, H. J. (2021). Preparation and characterization of surimi-based imitation crab meat using coaxial extrusion three-dimensional food printing. *Innovative Food Science & Emerging Technologies, 71*, Article 102711.
Kim, S. M., Wen, Y., Kim, H. W., & Park, H. J. (2022). Textural and sensory qualities of low-calorie surimi with carrageenan inserted as a protein substitute using coaxial extrusion 3D food printing. *Journal of Food Engineering, 111141*.
Ko, H. J., Wen, Y., Choi, J. H., Park, B. R., Kim, H. W., & Park, H. J. (2021). Meat analog production through artificial muscle fiber insertion using coaxial nozzle-assisted three-dimensional food printing. *Food Hydrocolloids, 120*, Article 106898.
Kong, D., Zhang, M., Mujumdar, A. S., & Li, J. (2023). Feasibility of hydrocolloid addition for 3D printing of Qingtuan with red bean filling as a dysphagia food. *Food Research International, 112469*.
Kouzani, A. Z., Adams, S., Whyte, D. J., Oliver, R., Hemsley, B., Palmer, S., & Balandin, S. (2017, January). 3D printing of food for people with swallowing difficulties. In: *DesTech 2016: proceedings of the international conference on design and technology* (pp. 23–29). Knowledge E.
Kyriakopoulou, K., Dekkers, B., van der Goot, A. J. (2019). Plant-based meat analogues. In: *Sustainable meat production and processing* (pp. 103–126). Elsevier: Amsterdam, The Netherlands. ISBN 9780128148747.
Lanier, T. C., Carvajal, P., & Yongsawatdigul, J. (2005). Surimi gelation chemistry. *Surimi and Surimi Seafood, 2*, 436–489.
Li, J., Desam, G. P., Narsimhan, V., & Narsimhan, G. (2021). Methodology to predict the time-dependent storage modulus of starch suspensions during heating. *Food Hydrocolloids, 113*, Article 106463.
Liu, Z., Dick, A., Prakash, S., Bhandari, B., & Zhang, M. (2020). Texture modification of 3D printed air-fried potato snack by varying its internal structure with the potential to reduce oil content. *Food and Bioprocess Technology, 13*(3), 564–576.
Liu, Z., Zhang, M., & Yang, C. H. (2018). Dual extrusion 3D printing of mashed potatoes/strawberry juice gel. *Lwt, 96*, 589–596.
Lu, Z. H., Donner, E., Yada, R. Y., & Liu, Q. (2016). Physicochemical properties and in vitro starch digestibility of potato starch/protein blends. *Carbohydrate Polymers, 154*, 214–222.
Marouene, Z., Gardan, J., Lafon, P., Makke, A., Labergere, C., & Recho, N. (2021). A finite element method to predict the mechanical behavior of a pre-structured material manufactured by fused filament fabrication in 3D printing. *Applied Sciences, 11*, 5075.
Montoya, J., Medina, J., Molina, A., Gutiérrez, J., Rodríguez, B., & Marín, R. (2021). Impact of viscoelastic and structural properties from starch-mango and starch-arabinoxylans hydrocolloids in 3D food printing. *Additive Manufacturing, 39*, Article 101891.
Najjar, R. S., & Feresin, R. G. (2019). Plant-based diets in the reduction of body fat: Physiological effects and biochemical insights. *Nutrients, 11*(11), 2712.
Osen, R., Toelstede, S., Wild, F., Eisner, P., & Schweiggert-Weisz, U. (2014). High moisture extrusion cooking of pea protein isolates: Raw material characteristics, extruder responses, and texture properties. *Journal of Food Engineering, 127*, 67–74.
Patraşcu, L., Banu, I., Vasilean, I., & Aprodu, I. (2016). Rheological and thermo-mechanical characterization of starch–protein mixtures. *Agriculture and Agricultural Science Procedia, 10*, 280–288.
Pisano, A. (2021). Toothpaste, sea deeps, and invasive pressure monitoring: Stevin's law and Pascal's principle. In *Physics for Anesthesiologists and Intensivists* (pp. 99–109). Cham: Springer.
Prithviraj, V., Thangalakshmi, S., Arora, V. K., & Liu, Z. (2022). Characterization of rice flour and pastes with different sweeteners for extrusion-based 3D food printing. *Journal of Texture Studies*.
Rowat, S. J., Legge, R. L., & Moresoli, C. (2021). Plant protein in material extrusion 3D printing: Formation, plasticization, prospects, and challenges. *Journal of Food Engineering, 308*, Article 110623.
Saget, S., Costa, M., Santos, C. S., Vasconcelos, M. W., Gibbons, J., Styles, D., & Williams, M. (2021). Substitution of beef with pea protein reduces the environmental footprint of meat balls whilst supporting health and climate stabilisation goals. *Journal of Cleaner Production, 297*, Article 126447.
Shahbazi, M., Jäger, H., Chen, J., & Ettelaie, R. (2021). Construction of 3D printed reduced-fat meat analogue by emulsion gels. Part II: Printing performance, thermal, tribological, and dynamic sensory characterization of printed objects. *Food Hydrocolloids, 121*, Article 107054.
Shi, Y., Tu, L., Yuan, C., Wu, J., Li, X., Wang, S., … Chen, X. (2022). Regulatory mechanisms governing collagen peptides and their 3D printing application for frozen surimi. *Journal of Food Science*.
Siacor, F. D. C., Chen, Q., Zhao, J. Y., Han, L., Valino, A. D., Taboada, E. B., … Advincula, R. C. (2021). On the additive manufacturing (3D printing) of viscoelastic materials and flow behavior: From composites to food manufacturing. *Additive Manufacturing, 45*, Article 102043.
Singh, M., Trivedi, N., Enamala, M. K., Kuppam, C., Parikh, P., Nikolova, M. P., & Chavali, M. (2021). Plant-based meat analogue (PBMA) as a sustainable food: A concise review. *European Food Research and Technology, 247*(10), 2499–2526.
Sriprablom, J., Luangpituksa, P., Wongkongkatep, J., Pongtharangkul, T., & Suphantharika, M. (2019). Influence of pH and ionic strength on the physical and rheological properties and stability of whey protein stabilized o/w emulsions containing xanthan gum. *Journal of Food Engineering, 242*, 141–152.
Sun, C., Fu, J., Chang, Y., Li, S., & Fang, Y. (2021). Structure design for improving the characteristic attributes of extruded plant-based meat analogues. *Food Biophysics*, 1–13.
Tan, M., Nawaz, M. A., & Buckow, R. (2021). Functional and food application of plant proteins–a review. *Food Reviews International*, 1–29.
Thangalakshmi, S., Arora, V. K., Kaur, B. P., Singh, R., Malakar, S., Rathi, S., & Tarafdar, A. (2022). Effect of steaming as postprocessing method on rice flour and Jaggery 3D printed construct. *Journal of Food Quality, 2022*, Article 3531711.
Theagarajan, R., Nimbkar, S., Moses, J. A., & Anandharamakrishnan, C. (2021). Effect of post-processing treatments on the quality of three-dimensional printed rice starch constructs. *Journal of Food Process Engineering, 44*(9), e13772.
Torres, M. D., Chenlo, F., & Moreira, R. (2018). Rheological effect of gelatinisation using different temperature-time conditions on potato starch dispersions: Mechanical characterisation of the obtained gels. *Food and Bioprocess Technology, 11*(1), 132–140.
Uribe-Wandurraga, Z. N., Zhang, L., Noort, M. W., Schutyser, M. A., García-Segovia, P., & Martínez-Monzó, J. (2020). Printability and physicochemical properties of microalgae-enriched 3D-printed snacks. *Food and Bioprocess Technology, 13*(11), 2029–2042.
Villanueva, M., Ronda, F., Moschakis, T., Lazaridou, A., & Biliaderis, C. G. (2018). Impact of acidification and protein fortification on thermal properties of rice, potato and tapioca starches and rheological behaviour of their gels. *Food Hydrocolloids, 79*, 20–29.
Wang, T., Kaur, L., Furuhata, Y., Aoyama, H., & Singh, J. (2022). 3D printing of textured soft hybrid meat analogues. *Foods, 11*(3), 478.
Wang, S., & Liu, S. (2021). 3D printing of soy protein-and gluten-based gels facilitated by thermosensitive cocoa butter in a model study. *ACS Food Science & Technology, 1*(10), 1990–1996.
Wang, L., Zhang, M., Bhandari, B., & Yang, C. (2018). Investigation on fish surimi gel as promising food material for 3D printing. *Journal of Food Engineering, 220*, 101–108.

Wild, F. (2016). Manufacture of meat analogues through high moisture extrusion. In: *Reference module in food science*.

Yang, F., Zhang, M., Bhandari, B., & Liu, Y. (2018). Investigation on lemon juice gel as food material for 3D printing and optimization of printing parameters. *Lwt, 87*, 67–76.

Yang, F., Zhang, M., Prakash, S., & Liu, Y. (2018). Physical properties of 3D printed baking dough as affected by different compositions. *Innovative Food Science & Emerging Technologies, 49*, 202–210.

Zahari, I., Ferawati, F., Helstad, A., Ahlström, C., Östbring, K., Rayner, M., & Purhagen, J. K. (2020). Development of high-moisture meat analogues with hemp and soy protein using extrusion cooking. *Foods, 9*(6), 772.

Zheng, Z., Zhang, M., & Liu, Z. (2021). Investigation on evaluating the printable height and dimensional stability of food extrusion-based 3D printed foods. *Journal of Food Engineering, 306*, Article 110636.

Zhu, Y., Lu, Y., Ye, T., Jiang, S., Lin, L., & Lu, J. (2021). The effect of salt on the gelling properties and protein phosphorylation of Surimi-Crabmeat mixed gels. *Gels, 8*(1), 10.